Barcelona-Catania-Paris-Madrid functional with a realistic effective mass

M. Baldo[*]
Instituto Nazionale di Fisica Nucleare, Sezione di Catania, Via Santa Sofia 64, I-95123 Catania, Italy

L. M. Robledo[†]
Departemento Física Teórica (Módulo 15), Universidad Autónoma de Madrid, E-28049 Madrid, Spain

P. Schuck[‡]
Institut de Physique Nucléaire, CNRS, UMR8608, F-91406 Orsay, France Université Paris-Sud, Orsay F-91505, France and Laboratoire de Physique et Modélisation des Milieux Condensés, CNRS et Université Joseph Fourier, 25 Av. des Martyrs, BP 166, F-38042 Grenoble Cedex 9, France

X. Viñas[§]
Departament d'Estructura i Constituents de la Matèria and Institut de Ciències del Cosmos, Facultat de Física, Universitat de Barcelona, Diagonal 647*, 08028 Barcelona, Spain*
(Received 5 April 2016; revised manuscript received 11 October 2016; published 18 January 2017)

The Barcelona-Catania-Paris-Madrid functional recently proposed to describe nuclear structure properties of finite nuclei is generalized as to include a realistic effective mass. The resulting functional is as good as the previous one in describing binding energies, radii, deformation properties, etc. In addition, the description of giant quadrupole resonance energies is greatly improved.

DOI: 10.1103/PhysRevC.95.014318

I. INTRODUCTION

In a recent paper [1], we developed an energy density functional theory for finite nuclei inspired by the Kohn-Sham (KS) approach where the bulk part was fitted to the microscopic results of Baldo *et al.* [2]. They were obtained with the Brueckner Hartree-Fock (BHF) approach including a three-body force taken from Ref. [3]. The interaction term of the equations of state (EOS) for symmetric nuclear and pure neutron matters were represented by polynomials of integer powers in the density supplemented by a quadratic interpolation for asymmetric matter. In this way, a very faithful representation of the microscopic energy per particle $E(\rho_p,\rho_n)/A$ as a function of proton (p) and neutron (n) densities was obtained for densities up to about three times saturation density (ρ_0). As discussed at length in Ref. [1] this work is part of an ongoing effort in the nuclear physics community to obtain energy density functionals applicable all over the nuclide chart and able to provide an accurate description of many nuclear properties—see Refs. [4–7] for some examples in different contexts. The functional of [1] has proven also to be useful in the description of the equation of state (EOS) of neutron stars from the outer crust to the core on a microscopical basis [8].

In order to account for finite nuclei where surface effects are relevant, a very simple Hartree type of term was added with a single Gaussian as effective central two-body force. Its strength was fixed from the first-order term of the polynomial fit and, thus, only one free parameter, the range, was left for adjustment. A second adjustable parameter was given by the strength $W_{\rm LS}$ of the spin-orbit force which was not extracted from the microscopic calculation though, in principle, this might be possible [9–11]. A third parameter came from the fact that the microscopic equilibrium value of the energy per particle had to be slightly renormalized by about 10^{-2} percent because in finite nuclei this value gets coupled with the surface energy. In this case, all coefficients of the polynomials in ρ_n,ρ_p have then been changed by the same factor. With only those three adjustable parameters, namely r_0, $W_{\rm LS}$, and E/A of the infinite system, the root mean square (rms) deviations from experimental masses and charge radii were 1.58 MeV and 0.027 fm, respectively [1]. An analogous procedure for constructing the functional was followed in Ref. [12]. A variant of this approach was adopted in Ref. [13], where a Skyrme force was derived from BHF calculations in nuclear matter, rather than directly the functional. A peculiarity of the Barcelona-Catania-Paris-Madrid (BCPM) functional is that, like in Ref. [12] but contrary to most of the Skyrme functionals, its effective mass m^* is equal to the bare one $m = m^*$. The question of effective mass is a quite subtle one. In principle there are two types of effective masses, the so-called k mass and the ω mass [14]. The k mass stems from the nonlocality and, thus, from the momentum (k) dependence of the static Hartree-Fock type of mean field which, to fix the ideas, may be derived from a Brueckner G matrix [15]. A typical value of the effective k mass is $m^* = 0.7m$. On the other hand the so-called ω mass is obtained in considering dynamic corrections to the single particle self-energy which lead to an energy ($\hbar\omega$) dependence. Most of the time a coupling of the single particle motion to higher configurations or to collective modes is

[*]marcello.baldo@ct.infn.it
[†]luis.robledo@uam.es
[‡]schuck@ipno.in2p3.fr
[§]xavier@ecm.ub.es

considered [14] and this compensates to a large percentage the reduction of the k mass with respect to the bare mass, so that the combined effect is that the total effective mass becomes close to the bare mass again. This effect, however, only holds for the states close to the Fermi energy whereas in the calculation of the ground state energy all configurations enter, so that a precise decision of whether one should take a reduced effective mass or not is difficult to make unless one really undertakes a reliable microscopic calculation for the ω mass and includes it in the self-consistent mean field cycle. This, however, tremendously complicates the whole approach. Anyway, it seems to be a fact that EDF's with or without reduced masses are about equally successful and it must be concluded that apparently the ambiguity of the effective mass can be very efficiently mocked up by a renormalization of finite size properties such as, e.g., the surface energy. On the other hand, for excited states the story can be different. The sensitivity to the effective mass depends on the multipolarity of the excitations. If the single particle self-energy is introduced, it should be taken off-shell and it is not straightforward to include an effective mass. Furthermore self-energy effects can be strongly compensated by vertex corrections, like the exchange of collective modes between the particle and the hole [16].

It is our intention in this work to extend our BCPM-EDF to include an effective density dependent mass which we extract again from the same G-matrix calculations [2,17] as it was done for the ground state energy. Also for proton and neutron effective masses we will adjust a polynomial fit in the density. The number of open parameters will stay the same as in the original BCPM-EDF. We shall call the new EDF BCPM*.

The paper is organized as follows. In Sec. II the methodology used to introduce a nonconstant effective mass in the BCPM functional is presented along with details on the calculation of finite nuclei. In Sec. III we present the results of the fit of the new functional to the rms deviation of binding energies. With the new set of parameters we have performed some nuclear structure calculations, like the evaluation of potential energy surfaces relevant to fission and the estimation of the excitation energies of giant monopole and giant quadrupole resonances.

II. METHODS

The BCPM energy density functional derived in Ref. [1] is inspired by the KS density functional theory [18]. Although the original KS theory is local, it has been extended to the nonlocal case, i.e., including effective mass and spin-orbit contributions (see Ref. [19] and references therein). Our functional uses a simple polynomial of the total density $\rho = \rho_n + \rho_p$ up to fifth order and of the asymmetry parameter $\beta = (\rho_n - \rho_p)/\rho$ up to second order, to fit the realistic equation of state of symmetric and neutron matters obtained with a state of the art microscopic calculation with realistic forces. We use the same polynomial for finite nuclei but this time in powers of the density of the finite nucleus

$$\rho(\vec{r}) = \sum_{ij} \phi_i^*(\vec{r})\rho_{ji}\phi_j(\vec{r}). \tag{1}$$

Here, the $\phi_i(\vec{r})$ are some basis wave functions (in our case, harmonic oscillator wave functions) and ρ_{ji} is the Hermitian density matrix. To incorporate other effects not present or difficult to address in nuclear matter like the spin-orbit interaction or surface energy repulsion, additional terms discussed below are incorporated into the functional. The kinetic energy is treated at the quantum mechanical level by introducing the kinetic energy density

$$\tau(\vec{r}) = \sum_{ij} \vec{\nabla}\phi_i^*(\vec{r})\rho_{ji}\vec{\nabla}\phi_j(\vec{r}). \tag{2}$$

The total energy of a finite nucleus is then given by

$$E = T + E_{int}^{\infty} + E_{int}^{FR} + E_{s.o.} + E_C, \tag{3}$$

where T is the kinetic energy,

$$E_{int}^{\infty} = \int d\vec{r}\,\rho(\vec{r})[P_s(\vec{r})(1-\beta^2(\vec{r})) + P_n(\vec{r})\beta^2(\vec{r})] \tag{4}$$

is the bulk energy, given in terms of the polynomials $P_s(\rho)$ and $P_n(\rho)$ for symmetric and neutron matter and the asymmetry density $\beta(\vec{r}) = (\rho_n(\vec{r}) - \rho_p(\vec{r}))/\rho(\vec{r})$, E_{int}^{FR} is a finite range surface term, $E_{s.o.}$ is the spin-orbit energy taken from the Skyrme or Gogny forces, and E_C is the standard Coulomb repulsion including the exchange energy in the Slater approximation, see [1] for a definition of the different terms. This energy is supplemented by a density-dependent zero-range pairing interaction. Finally, a rotational energy correction, relevant in deformed nuclei, is subtracted, see below.

The inclusion of an effective mass in BCPM is carried out by means of adding and subtracting an appropriate kinetic energy term to the original kinetic energy density

$$\frac{\hbar^2}{2m_q}\tau_q \to \frac{\hbar^2}{2m_q^*}\tau_q - B(\rho_q)\tau_q^{\infty} \tag{5}$$

with

$$\frac{\hbar^2}{2m_q^*}\tau_q = \frac{\hbar^2}{2m_q}\tau_q + B(\rho_q)\tau_q, \tag{6}$$

where $B(\rho_q) = \frac{\hbar^2}{2m_q}(m_q/m_q^* - 1)$. In this expression m_q^* is the coordinate dependent effective mass for protons $q = p$ or neutrons $q = n$, τ_q is the quantal kinetic energy density of Eq. (2) for each kind of nucleon, and τ_q^{∞} is the kinetic energy density in the uniform medium $\tau_q^{\infty} = \frac{3}{5}(3\pi^2)^{2/3}\rho_q^{5/3}(\vec{r})$. This substitution guarantees that the kinetic energy at nuclear matter level remains the same as before. With this redefinition of the kinetic energy the functional now reads

$$E = T^* + E_{int}^{\infty *} + E_{int}^{FR} + E_{s.o.} + E_C, \tag{7}$$

where

$$T^* = \sum_q \int d\vec{r}\,\frac{\hbar^2}{2m_q^*(\vec{r})}\tau_q(\vec{r}), \tag{8}$$

and $E_{int}^{\infty *}$ is obtained by subtracting

$$\sum_q B(\rho_q)\tau_q^{\infty} \tag{9}$$

from the energy E_{int}^{∞} given in Eq. (4). The rationale behind this procedure is to preserve the nuclear matter EoS of BCPM and, therefore, all the nuclear matter properties of this functional—see [1] for a discussion.

It should be noted that above functional is not gauge invariant, feature which should hold, if one treats rotating nuclei or other motions involving nonvanishing currents. Like for Skyrme forces, it is, however, easy to repair this deficiency. One indeed checks that the following replacement:

$$B\tau \rightarrow B(\tau - \mathbf{j}^2/\rho) \tag{10}$$

with $\mathbf{j}$ the current, makes this piece of the functional gauge invariant. One realizes that for the case of Skyrme forces $B \propto \rho$ and, thus the usual combination $\rho\tau - \mathbf{j}^2$ is recovered. It is evident that all the properties and consequences of a gauge invariant functional, amply studied in the case of Skyrme forces [20,21], can be taken over to our case. This concerns, for instance, the gauge invariant rewriting of the spin-orbit term [20,21]. Also the finite range surface term is gauge invariant, since it is of the Hartree-type, see [20]. Therefore with Eq. (10) the whole BCPM* functional is easily written in a moving frame, since Galilean invariance is just a special case of a general local gauge transformation.

Pairing correlations, required to describe open shell nuclei, are introduced by means of a density-dependent zero-range force of the type suggested by Bertsch and Esbenssen [22]

$$V_{\text{Pair}}(\vec{r}_1,\vec{r}_2) = V_0\left\{1 - \eta\left[\rho\left(\frac{\vec{r}_1+\vec{r}_2}{2}\right)\Big/\rho_0\right]^{\alpha}\right\}\delta(\vec{r}_1 - \vec{r}_2). \tag{11}$$

This force is widely used in nuclear structure calculations [23] including the BCPM functional [2,24]. The parameters $V_0 = -481$ MeV fm^3, $\eta = 0.45$, the saturation density $\rho_0 = 0.16$ fm^{-3}, and $\alpha = 0.47$ are taken from [23] and correspond to a fit of the nuclear matter pairing gap of Gogny D1 with an effective mass of 0.67. Although our effective mass at saturation is higher (see below) we have preferred to keep the present parametrization of the pairing interaction for consistency with BCPM. The same energy window of 60 MeV from the bottom of the HF potential as in [23] has been used in the present calculation.

The two-body kinetic energy correction, which accounts for the lack of translational invariance, is taken as in [1]. The final ingredient of the energy is the rotational energy correction ϵ_{rot} which is estimated using the rotational approximation $\epsilon_{\text{rot}} = \langle \Delta \vec{J}^2 \rangle/(2\mathcal{J}_Y)$ defined in terms of the Yoccoz moment of inertia $\mathcal{J}_Y$ [25] and computed using the HFB like intrinsic wave function corresponding to the variational minimum of the HFB energy. This rotational correction is subtracted from the functional's energy in the spirit of the projection after variation (PAV) method applied to rotational symmetry restoration—see [25–27] for a thorough overview of the method. Note that the rotational energy correction plays an important role in deformed nuclei and its inclusion is relevant to describe masses along the whole periodic table. In strongly deformed midshell heavy nuclei the rotational energy correction can reach values as large as 6 or 7 MeV. This correction, however, is almost negligible in magic or semimagic nuclei, which are basically spherical. Due to the fact that the spherical-deformed transition is sharp, the rotational correction goes from zero to some MeV at the transition point leading to sharp variations in the binding energy plot—see below.

The finite nuclei calculations have been carried out with an adapted HFBAXIAL [28,29] computer code preserving axial symmetry. The quasiparticle operators are expanded in a three-dimensional axially symmetric harmonic oscillator basis with varying number of oscillator shells depending on mass number as to guarantee a weak dependence of binding energies with the basis size. In [1] we used a phenomenological formula to extrapolate binding energies to the value corresponding to an infinite size HO basis. As this phenomenological procedure has proven in our case to lead to some difficulties for weakly deformed or shape coexisting nuclei and it has been recently questioned [30], we have preferred to change our computational strategy by increasing the basis size used in Ref. [1]. In order to study the impact of truncation errors in the absolute binding energies and the parameter fit, we have defined three basis sets. In the first set (basis 1) the size of the bases used are 15 major shells for $Z \leqslant 50$, 17 major shells for $52 \leqslant Z \leqslant 82$, and 19 major shells for $84 \leqslant Z \leqslant 110$. The next two sets are obtained by increasing by two shells (basis 2) and four shells (basis 3) the bases in each Z interval. The oscillator basis preserves axial symmetry and therefore depend upon two oscillator lengths $b_\perp$ and b_z. In principle, those two lengths should adapt to the geometry of the nucleus as to minimize the energy. However, given the large number of shells used in the three basis sets and the relatively small typical value of the β_2 quadrupole deformation parameter encountered in the ground state of atomic nuclei (typically less than 0.35 in absolute value) we have considered more practical to keep them equal ($b_\perp = b_z = b$) for the binding energy calculations used to fit the parameters of the functional. The oscillator length b of the basis depends on mass number and the traditional $b = A^{1/6}$ (in fm) formula found in any nuclear physics textbook, sometimes with slightly different numerical factors, has been used. In this way a costly nucleus by nucleus optimization is avoided. The error induced by this simplification is not relevant given the large size of the basis. With this set up, all quantities depending on energy differences, like one or two neutron separation energies, α decay Q values, etc., are expected to converge to less than 50 keV for most of the nuclei considered as verified by comparing the S_{2n} values obtained with basis 2 and basis 3. These results concerning the convergence of S_{2n} with the basis size are in consonance with the findings in [30] as shown in their Fig. 11.

Only even-even nuclei have been considered in the present study as the proper treatment of odd nuclei will require a HFB plus blocking scheme that implies the consideration of the "time odd" sector of the functional. This sector is not easily fixed by nuclear matter properties and only affects very weakly bulk properties like binding energies (the only quantity used to fix the functional) or radii. Odd nuclei were neither considered in Ref. [1].

The effective masses m_n^* and m_p^* for neutrons and protons are obtained in the uniform system in terms of the neutron and proton single particle potentials U_n and U_p, calculated within the Brueckner-Hartree-Fock (BHF) procedure. At the Fermi

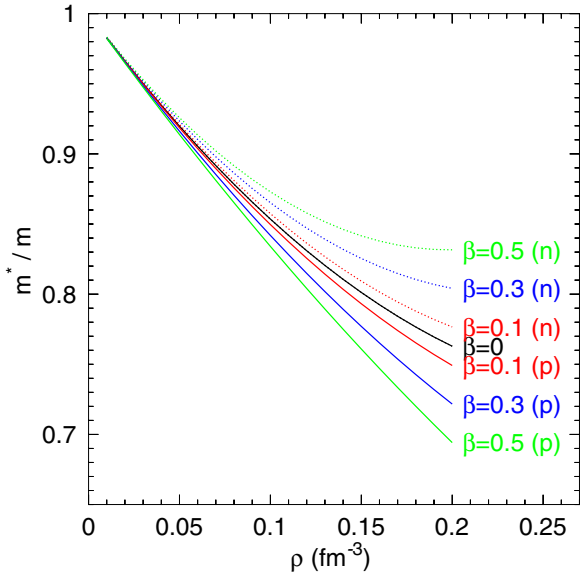

FIG. 1. Proton (p, full line) and neutron (n, dotted line) effective masses corresponding to the linear fit of Eq. (13) are plotted as a function of the density for different values of the isospin asymmetry parameter β.

momenta k_{Fq} one has

$$\frac{m_q}{m_q^*} = 1 + \frac{m_q}{\hbar^2 k_{Fq}} \left(\frac{dU_q(k)}{dk} \right)_{k=k_{Fq}}, \tag{12}$$

where $q = n$, p and m_q is the bare nucleon mass. The effective mass is a function both of the total density ρ and of the asymmetry $\beta = (\rho_n - \rho_p)/\rho$.

We used Eq. (12) in a systematic calculation of the neutron and proton effective masses for a set of total densities, ranging from 0 to 0.2 fm^{-3}, and asymmetries β from 0 to 1. We found that the neutron and proton effective masses can be fitted by a simple polynomial expression

$$\frac{m_n^*}{m_n} = a_0(\rho) + a_1(\rho)\beta; \qquad \frac{m_p^*}{m_p} = a_0(\rho) - a_1(\rho)\beta, \tag{13}$$

where

$$a_0 = 1 - 1.744025\rho + 2.792075\rho^2,$$
$$a_1 = 0.090795\rho + 2.981724\rho^2 \tag{14}$$

are dimensionless parameters depending on the density ρ. For this expression to make sense the density ρ has to be given in units of fm^{-3}. Taking saturation density as $\rho_{\rm sat} = 0.16\,{\rm fm}^{-3}$ we get from the above fit the values $m_n^*/m_n = m_p^*/m_p = 0.79$ for $\beta = 0$.

This expression can be extended to negative values of β, provided we simply interchange neutrons and protons, as it must be. Since the neutron and proton effective masses have a symmetric splitting, see Eq. (13) and Fig. 1, they have a continuous derivative at $\beta = 0$. A closer comparison with the microscopic results reveals that the fit with a linear dependence on β looks not enough for the whole range up to $\beta = 1$ (pure neutron matter). Although the deviations could be taken into account by introducing higher powers in β, the linear fit is good up to values of $\beta \approx 0.5$, which are within the range of values appearing in stable nuclei, with the exception of very light nuclei, for which the BCPM functional is not expected to be applicable. Therefore, we keep the fit of Eqs. (13) and (14) neglecting the deviations, which can appear at very large asymmetries. We are aware, however, that in situations of large asymmetry, like in Wigner-Seitz cells in neutron stars, our simple linear dependence will not be enough. In Ref. [31] the neutron to proton mass splitting is expressed as $(m_n^* - m_p^*)/m = (0.27 \pm 0.25)\beta$, while more recently [32] a similar analysis gives $(0.41 \pm 0.15)\beta$. From Eq. (14) at saturation one finds 0.18β for BCPM*, i.e., a splitting that agrees in the sign but it appears to be on the small side. In any case one should appreciate the rough agreement between phenomenology and theory what is not obvious nor trivial and is not found in most parametrizations of the Skyrme or Gogny functionals. In finite nuclei the polynomial fit in Eq. (13) is maintained but using the finite nucleus density instead of the nuclear matter one.

III. RESULTS

In this section we discuss first the fitting of the free parameters of the BCPM* functional to minimize the rms binding energy difference with the experimental data. The functional so obtained is then used to carry out calculations to asset its merits regarding quadrupole deformation properties and excitation energies of giant resonances.

A. Binding energies and radii

As a consequence of the introduction of the effective mass in finite nuclei, a readjustment of some of the parameters of BCPM is required. The most affected is the spin-orbit interaction strength, which is inversely proportional to the effective mass and, therefore, is going to have a value in BCPM* closer to the value of other functionals like Gogny D1S or D1M with effective masses not equal to the bare one. The reason for such dependence is the link between the spin-orbit strength and the magic numbers: $W_{\rm LS}$ has to be large enough as to bring intruder orbital down to the lower major shell. Decreasing the effective mass increases the gap between major shells and, therefore, a larger $W_{\rm LS}$ value is required. The spin-orbit strength along with the other two range parameters r_{0L} and r_{0U} (see [1] for more information) are readjusted as to fit the binding energies of spherical and deformed even-even nuclei in a similar manner as in [1]. As a first step we carried out a comprehensive study with the basis 1 set (see above for the definition) in order to find the optimal values of the parameters minimizing the rms for the binding energy difference using the AME 2012 experimental compilation including 620 even-even nuclei [33]. The rms value obtained in this way is $\sigma_{\rm E} = 1.65$ MeV which is slightly higher than the original BCPM value of 1.58 MeV obtained with only 579 even-even nuclei (1.61 MeV when the AME 2012 compilation is considered). The values of the fitted parameters are $r_{0U} = r_{0L} = 0.7520$ fm and $W_{\rm LS} = 112$ MeV fm^5. We

observe that as in the BCPM case, the minimization of the binding energy favors equal values of the r_{0U} and r_{0L} ranges. Concerning the binding energy per nucleon E/A in nuclear matter, the same value as in BCPM, namely 15.98 MeV, yields the lowest binding energy rms. Due to the truncation error induced in the binding energies by using a finite dimensional basis the previous values of the parameters are linked to the basis set used. In order to explore the dependency of the parameters with the basis size and to assess the convenience of the basis sets used we have performed calculations with the basis sets 2 and 3 which include many more HO states. Given the weak dependence of $\sigma_{\rm E}$ with the spin-orbit strength and E/A in nuclear matter we have kept them fixed in this study and only the parameter $r_{0U} = r_{0L} = r_0$ has been explored. The quantity r_0 has been explored in steps of 0.0005 fm around the initial value. The results indicate that for the basis 2 calculation the optimal r_0 value keeps its original value of 0.7520 fm with $\sigma_E = 1.63$MeV. In the case of basis 3 (23 HO shells in the actinides) the optimal r_0 value is 0.7525 and σ_E slightly increases to 1.65 MeV. The weak variation of r_0 and the constancy of σ_E points to a good convergence of relative binding energies already for basis 1. It also points to the fact that in a global fit, what is slightly worsened in a region of the periodic table can be compensated by slight improvements in another region.

More insight is gained by looking at the specific behavior of the binding energy difference as a function of neutron number for each of the Z values considered. Those quantities, as obtained with basis 3 are plotted in Fig. 2 (see figure caption for an explanation of the different elements in the plot). In this plot we observe a nice reproduction of experimental data for heavy nuclei away from magic or semimagic numbers. Close to magic numbers we observe in many cases a nonsmooth behavior which is due, as explained in [1], to a deficiency on the way the rotational energy correction used in the definition of the binding energy is computed: As mentioned in the previous section, the rotational energy correction is obtained using the intrinsic wave function minimizing the HFB energy and, therefore, it is zero for spherical intrinsic states. The correction suddenly jumps by a couple of MeV when the spherical to deformed transition takes place and the jump obviously reflects in the binding energy. This deficiency could be cured by computing the rotational energy correction in the variation after projection (VAP) scheme but this procedure, even in an approximate way, is much more costly to implement than the present method. Work to find a convenient way to implement the VAP is under way. We also observe that, for light nuclei the agreement with the experimental binding energies deteriorates and the dependence with proton and neutron number is not well reproduced. This is a common feature of many (if not all) functionals, including BCPM. The value of $\sigma_{\rm E}$ obtained with BCPM and BCPM* is comparable to the one of many Skyrme, Gogny, or relativistic functionals. However it cannot compete with some models like HFB-21 [7] or Gogny D1M [5] that include beyond mean field effects and more phenomenological ingredients.

The onset of deformation can be easily seen in the figure because deformed nuclei correspond to those nuclei with a nonzero rotational correction. Spherical nuclei are obtained near or at magic neutron or proton numbers while quadrupole deformed ground states are obtained otherwise.

Concerning charge radii we have also computed the rms deviation σ_R with respect to the 315 experimental data points corresponding to even-even nuclei and published in the recent compilation of Angeli *et al.* [34]. The theoretical radius is computed using the standard formula $r_{\rm ch} = \sqrt{\langle r^2\rangle_{\rm HFB} + 0.875^2}$. The value obtained for σ_R using the BCPM* functional is $\sigma_R = 0.024$fm, which is around 15% better than the 0.027 fm value obtained with BCPM. In Fig. 3 we plot the difference between the theoretical and experimental value of the charge radii as a function of the mass number A for the 315 even-even nuclei with experimentally known charge radii [34]. Overall, we see a very good agreement with experimental data, except in some superheavy and light nuclei. These deficiencies were also observed in the BCPM results of Ref. [1].

To summarize our findings, we present in Table I the values of the BCPM* parameters along with the ones of BCPM. In the table the rms of the binding energy and radii differences and corresponding to even-even nuclei are also given.

As the nuclear matter EoS of BCPM has been preserved in BCPM*, all its nuclear matter parameters K, J, etc., remain exactly the same as with BCPM and we refer the reader to Ref. [1] for an extensive discussion of their values. In addition, the BCPM* values of the range parameters of the surface term have not changed substantially, with respect to the ones of BCPM and, therefore, it is to be expected that the variance analysis of σ_E with respect to the parameters r_{0L}, r_{0U}, and $W_{\rm LS}$ carried out in [1] is going to yield similar conclusions for BCPM*.

B. Fission barrier heights

A fundamental aspect of any nuclear effective interaction is its ability to produce reasonable deformation properties. For this reason, we studied in Refs. [35,36] the quadrupole and octupole deformation properties of some selected nuclei as provided by the BCPM energy density functional and found a good agreement with other well reputed functionals like Gogny D1S [37]. On the other hand, the fission phenomenon, which is described as the collective evolution of the nucleus from its ground state to scission using the quadrupole deformation parameter as driving coordinate, is perhaps the best testing ground for deformation properties as it results from a subtle competition between surface tension and Coulomb repulsion. From the perspective of comparing with experimental data, there are well established values of the fission barrier heights in a number of actinides and super-heavies that could be used. Those values are extracted in a model dependent way from the behavior of the induced fission cross section as a function of the energy and are routinely used as benchmarks of theoretical fission models. In previous studies [38,39] we have shown that the BCPM interaction produces quite reasonable results for fission observables and, in any case, as good as the ones obtained with other functionals including fission data in their fitting protocols [40]. Therefore, we have repeated some of the calculations to evaluate the impact of the effective mass on those observables. In order to obtain barrier heights, the computation of the energy landscape as a function of

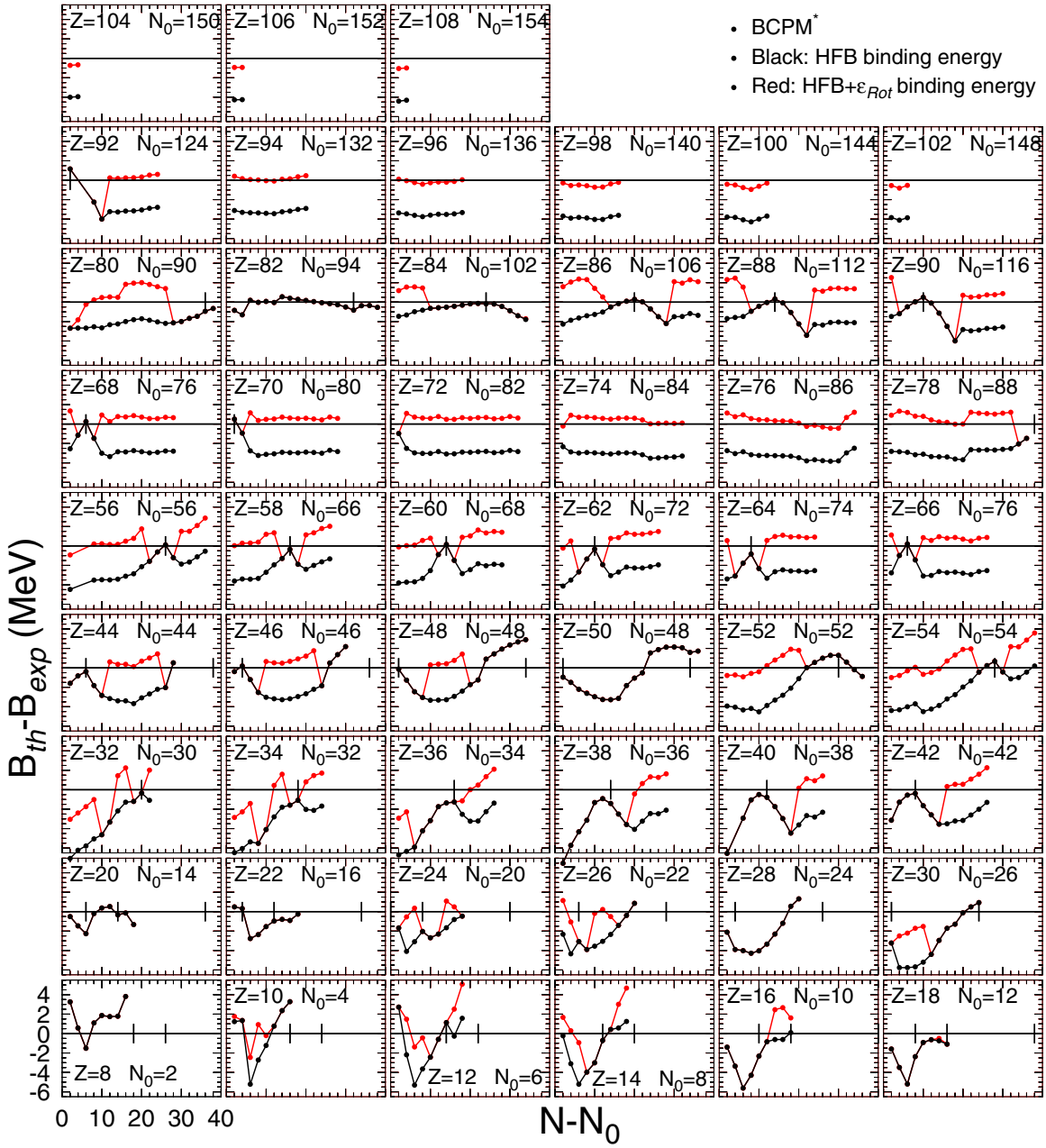

FIG. 2. Binding energy difference $\Delta B = B_{\rm th} - B_{\rm exp}$ (MeV) as a function of the shifted [by $N_0(Z)$] neutron number $N - N_0(Z)$. The values of Z and the neutron number shift $N_0(Z)$ are given in each panel. In all the panels the ordinate ΔB axis ranges from -6.5 MeV to 5.5 MeV with long ticks at -6, -4, etc., MeV. The $N - N_0(Z)$ axis spans a range of 40 units with long ticks every ten units and short ones every two units. For instance, for the nucleus of ^{132}Ce ($Z = 58$, $N = 74$) the value of N_0 is 66 and therefore $N - N_0 = 8$. In every panel, a horizontal line corresponding to $\Delta B = 0$ has been plotted to guide the eye. Additional perpendicular lines signaling the position of magic neutron numbers have also been included. Black curves correspond to theoretical binding energies computed with the HFB method whereas the red curves additionally include the rotational energy correction $\epsilon_{\rm rot}$ discussed in the text. The HFB calculations have been carried out with the basis 3 set.

the quadrupole moment is required. In this case and due to the variety of shapes involved the HO basis used has to be redefined as to include many more HO shells (26 shells) in the z direction. In addition, to minimize truncation errors in the deformation energies a careful optimization of the oscillator length parameters is carried out at each value of the quadrupole moment considered, see [41] for a convergence study. An example of such kind of calculations is shown in Fig. 4 using the paradigmatic case of ^{240}Pu. For comparison, the results obtained with BCPM and with the Gogny D1S functional [37] are also plotted. The potential energy is given by the HFB one including the standard rotational energy correction $\epsilon_{\rm rot} = \langle \Delta \vec{J}^2 \rangle / (2\mathcal{J}_{\rm Y})$ [25]. The results for the three functionals show a very similar behavior, with the position of maxima and minima being almost the same in the three cases. It is remarkable to notice the shoulder obtained with both BCPM

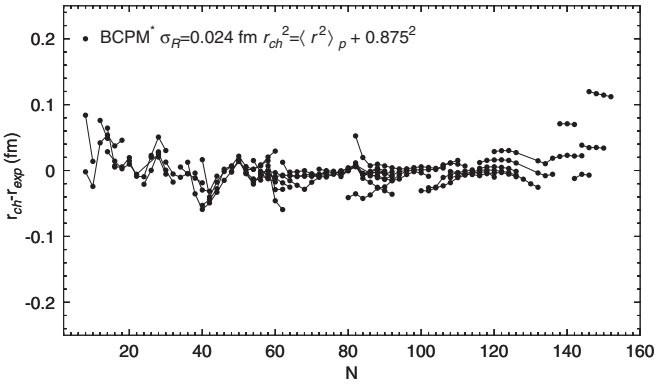

FIG. 3. The experiment-theory deviation $r_{\rm ch} - r_{\rm exp}$ for the 315 even-even nuclei with known experimental data [34] is plotted as a function of mass number A.

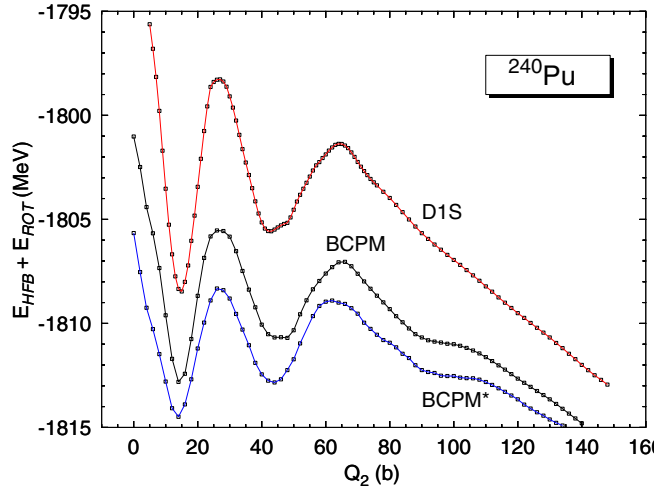

FIG. 4. Potential energy surface for fission, including the rotational energy correction, computed as a function of the quadrupole moment (in units of $b = 100$ fm^2) for the Gogny D1S, BCPM, and BCPM* functionals.

and BCPM* at $Q_{20} = 90$ b which is reminiscent of a second isomeric well. The connection of this shoulder with the second isomeric well observed in some U and Th isotopes deserves further investigation. The values obtained for the two barrier heights are given in Table II along with the corresponding numbers for ^{234}U, ^{244}Pu, ^{242}Cm, and ^{246}Cm and compared with experimental data.

We observe that both the results obtained with BCPM* as well as the ones with BCPM are in quite good agreement with experimental data [42], the ones obtained with BCPM* being slightly better. The results can not be taken as conclusive because triaxiality is not allowed to develop in the first barrier. However, the agreement of the calculations with experimental data for the second barrier is very encouraging as, in this case, triaxiality has proven to play a marginal role. The other observable quantity relevant in fission studies is the excitation energy of the fission isomer E_I which is also given in the table along with the existing experimental data for ^{240}Pu and ^{242}Cm. The theoretical predictions are lower than the experimental value by around 25% in the BCPM case and 40% with the new BCPM*.

In the five cases studied, reflection symmetry is broken for quadrupole moments beyond the second fission barrier. The behavior and values of the octupole moment for those configurations are very similar to the ones obtained with BCPM [38] and Gogny D1S, indicating that the good octupole properties of those functionals [36,43] are preserved in the present proposal. Work to analyze in more detail deformation properties of BCPM* is in progress and will be reported elsewhere.

C. Monopole and quadrupole giant resonance energies

In our previous work we have discussed with some detail the excitation properties of the BCPM energy density functional. In particular, we analyzed the excitation energies of the scalar giant monopole and quadrupole resonances (GMR and GQR, respectively) following the sum rule approach described in Ref. [44]. In this reference the m_1 and m_3 sum rules are obtained for Skyrme forces, but its calculation can be easily generalized to the BCPM and BCPM* cases. The m_1 sum rules are given by $m_1^M = (2\hbar^2/m)A\langle r^2\rangle$ and $m_1^Q = (4\hbar^2/m)A\langle r^2\rangle$, for the isoscalar monopole and quadrupole, respectively. Those expressions are valid in the case of gauge invariant Skyrme functionals as well as with the BCPM* functional using the gauge invariant expression (10), see, e.g., [45]. Then the previous expressions for the m_1 sum rules are recovered, as discussed in [46]. The m_3 sum rule is computed at $1p1h$ RPA

TABLE I. Values of the free parameters of BCPM [1] and BCPM* (this work) as determined by minimizing the rms of the binding energy difference of even-even nuclei using the AME 2012 compilation [33]. The σ_E value is given along with the corresponding value of the rms deviation of the radii. The results are obtained with basis 1 (see text) and only a weak dependence of the $r_{0U} = r_{0L} = r_0$ parameter is observed when increasing basis size (see text for details).

	W_{LS} (MeV fm^5)	r_{0U} (fm)	r_{0L} (fm)	E/A (MeV)	σ_E (MeV)	σ_R (fm)
BCPM	90.5	0.659	0.659	15.98	1.61	0.027
BCPM*	112	0.7520	0.7520	15.98	1.65	0.024

TABLE II. First (E_A) and second (E_B) fission barrier heights and the excitation energy of the fission isomer (E_I) are given in MeV for five typical actinide nuclei. Results obtained with BCPM* and BCPM are given along with the experimental data from [42].

	BCPM*			BCPM			Exp		
	E_A	E_B	E_I	E_A	E_B	E_I	E_A	E_B	E_I
^{234}U	5	5.8	1.8	5.6	5.6	2.	4.8	5.5	–
^{240}Pu	6.2	5.5	1.7	7.3	5.8	2.1	6	5.15	2.8
^{244}Pu	6.1	6.2	1.7	7.8	6.4	2.5	5.70	4.85	–
^{242}Cm	6.3	4.3	1.1	7.4	4.5	1.5	6.65	5.0	1.9
^{246}Cm	6.5	4.7	1.1	8	5.5	2.1	6	4.8	–

TABLE III. Theoretical E_3 and E_1 estimates (in MeV) of the average excitation energy of the GMR including pairing correlations. The E_3 estimate of the GQR, including pairing, is also displayed. The experimental energy of the centroid and the corresponding error for the GMR and GQR are given as well.

Nucleus	$E_3(M)$	$E_1(M)$	$E_3(Q)$	Exp(M)	Exp(Q)
^{90}Zr	19.10	18.31	14.65	17.81 ± 0.32	14.30 ± 0.40
^{144}Sm	16.45	15.66	12.59	15.40 ± 0.30	12.78 ± 0.30
^{208}Pb	14.53	13.89	11.18	13.96 ± 0.20	10.89 ± 0.30
^{112}Sn	17.73	16.96	13.64	16.1 ± 0.1	13.4 ± 0.1
^{114}Sn	17.62	16.85	13.56	15.9 ± 0.1	13.2 ± 0.1
^{116}Sn	17.50	16.81	13.48	15.8 ± 0.1	13.1 ± 0.1
^{118}Sn	17.39	16.70	13.41	15.6 ± 0.1	13.1 ± 0.1
^{120}Sn	17.28	16.59	13.34	15.4 ± 0.2	12.9 ± 0.1
^{122}Sn	17.18	16.39	13.28	15.0 ± 0.2	12.8 ± 0.1
^{124}Sn	17.08	16.28	13.22	14.8 ± 0.2	12.6 ± 0.1
^{106}Cd	18.01	17.16	13.87	16.50 ± 0.19	
^{110}Cd	17.74	16.89	13.68	16.09 ± 0.15	13.13 ± 0.66
^{112}Cd	17.61	16.85	13.59	15.72 ± 0.10	
^{114}Cd	17.48	16.65	13.50	15.59 ± 0.20	
^{116}Cd	17.36	16.53	13.42	15.40 ± 0.12	12.50 ± 0.66

level using the scaling approach [44,46]. Finally, we shall point out that, as far as we will describe only even-even nuclei, the time-odd quantities (i.e., currents) in the energy density, needed in general to recover the m_1 sum rule, will not give any contribution to the above considered sum rules due to the time-reversal symmetry in even-even nuclei [44,45]. Let us mention again here that all properties and technicalities of the Skyrme functionals concerning static and/or dynamic properties of nuclei, studied since several decades [20,21] can directly be taken over to the BCPM* functional. The only difference is that the function $B(\rho)$ is linear in ρ in the case of Skyrme and more complicated in the case of BCPM*.

We found that the BCPM predictions for the excitation energies of the GMR are in agreement with the results provided by other mean field models, nonrelativistic and relativistic, with a similar value of the incompressibility modulus K. However, it was found that the experimental excitation energies of the GQR were systematically underestimated by about 1 MeV. The underlying reason for that was that in BCPM the effective mass equals the bare one and it is known that the GQR excitation energies are sensitive to the value of the effective mass. We have repeated these calculations in the present work using the BCPM* energy density functional. In Table III we report the theoretical estimates of the excitation energy of the GMR and GQR, computed with our new functional, of a selected set of nuclei, for which the GMR excitation energy is experimentally known.

Comparing with Table VII of [1], one can see that the influence of the effective mass on the excitation energy of the GMR is basically negligible, while it is noticeable in the case of the GQR. This behavior can be understood in the scaling approach as follows. The scaled m_3 sum rules for the GMR and the GQR (see Eqs. (A12) and (A17) of [1]) contain a kinetic energy contribution coming from the second derivative of the scaled energy density respect to the scaling parameter

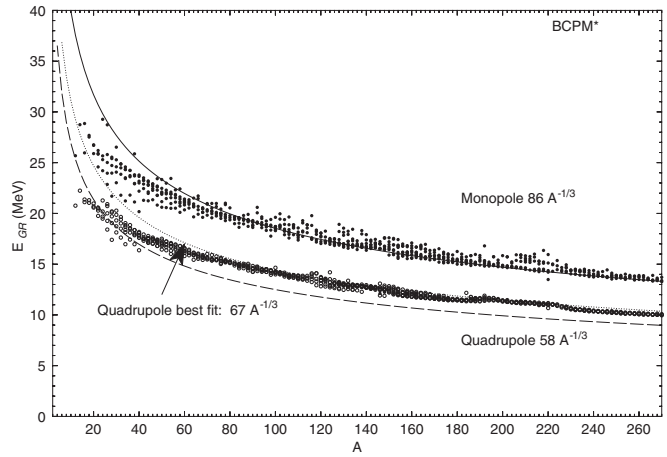

FIG. 5. Excitation energies of the monopole and quadrupole giant resonances as a function of mass number A obtained with the scaling approximation. The estimation $58A^{-1/3}$ for the quadrupole and $86A^{-1/3}$ for the monopole [25] are drawn to guide the eye. The dotted curve $67A^{-1/3}$ corresponds to the best fit of the quadrupole excitation energy.

λ. According to the transformation of Eq. (5), used in BCPM* to account for the kinetic energy, it is easy to see that both contributions τ and τ^∞ scale as λ^2 in the monopole case while in the quadrupole one only τ, given by Eq. (2), contributes as a consequence of volume conservation in the quadrupole oscillation. As far as in BCPM* the effective mass m^* is smaller than the bare mass m, the m_3 value and the excitation energy of the GQR $E_3(Q)$ will be larger than the predictions of the BCPM functional where $m^* = m$. Therefore, the agreement with the experimental values of the excitation energy of the GQR is better when computed with the BCPM* functional, as it can be seen in Table II.

In Fig. 5 we display the excitation energies of the monopole and quadrupole oscillations along the whole periodic table. Both follow a $C\,A^{-1/3}$ law with coefficients $C_M = 86$ and $C_Q = 67$ MeV, respectively. These values are roughly in agreement with the empirical values given in [25] of 86 and 58 MeV for the monopole and quadrupole resonances.

IV. CONCLUSIONS

In this work we propose a variant of the BCPM energy density functional published in [1], where the bare mass is replaced by a density dependent effective mass m^*. Though it may not be absolutely clear whether bare or effective mass is preferable as we argued in the Introduction, it is certainly true that for, e.g., giant resonances other than monopole and dipole ones an effective mass $m^* < m$ is favored. Again we used our strategy and deduced the effective mass from our microscopic G-matrix results and adjusted separately proton and neutron effective masses to our results of the Bruckner G matrix using polynomials in the density. A linear interpolation between proton and neutron effective masses was fitted to the asymmetries prevailing in finite nuclei. It turns out that the difference of both masses is quite a bit on the lower side of what one generally finds in the literature. In finite nuclei the

densities are then replaced by the local ones as obtained from the HFB calculation. Some parameters have to be readjusted, in first place this concerns the strength of the spin-orbit term, which now has values much closer to the usual values of Skyrme or Gogny functionals. Concerning the results, not surprisingly, the ones for the giant quadrupole resonance are now in significantly better agreement with experimental data. Fission barriers from BCPM* are slightly better than those with BCPM. On the other hand the excitation energy of the fission isomer is slightly worse with BCPM* than with BCPM when compared to the data for ^{240}Pu and ^{242}Cm. The rms value for the binding energy is 1.65 MeV with BCPM* and 1.61 MeV with BCPM, the rms value for the radii is 0.024 fm instead of 0.027 fm. All in all it can be said that BCPM* practically performs as well as BCPM for all quantities besides for the GQR where it yields sensitively better results.

ACKNOWLEDGMENTS

Work supported in part by the Spanish MINECO Grants No. FPA2012-34694, No. FIS2012-34479, and No. FIS2014-54672; by the Consolider Ingenio 2010 programs MULTIDARK CSD2009-00064 and CPAN CSD2007-00042; by Project No. MDM-201-0369 of ICCUB from MINECO; and by Grant No. 2014SGR-401 from the Generalitat de Catalunya.

[1] M. Baldo, L. M. Robledo, P. Schuck, and X. Viñas, Phys. Rev. C **87**, 064305 (2013).
[2] M. Baldo, L. Robledo, P. Schuck, and X. Viñas, J. Phys. G Nucl. Part. Phys. **37**, 064015 (2010), and references therein.
[3] A. Akmal, V. R. Pandharipande, and D. G. Ravenhall, Phys. Rev. C **58**, 1804 (1998).
[4] M. Kortelainen, J. McDonnell, W. Nazarewicz, E. Olsen, P.-G. Reinhard, J. Sarich, N. Schunck, S. M. Wild, D. Davesne, J. Erler, and A. Pastore, Phys. Rev. C **89**, 054314 (2014).
[5] S. Goriely, S. Hilaire, M. Girod, and S. Perú, Phys. Rev. Lett. **102**, 242501 (2009).
[6] T. Niksic, D. Vretenar, and P. Ring, Phys. Rev. C **78**, 034318 (2008).
[7] S. Goriely, N. Chamel, and J. M. Pearson, Phys. Rev. Lett. **102**, 152503 (2009).
[8] B. K. Sharma, M. Centelles, X. Vinas, M. Baldo, and G. F. Burgio, Astron. Astrophys. **584**, A103 (2015).
[9] R. R. Scheerbaum, Nucl. Phys. A **257**, 77 (1976).
[10] M. Kohno, Phys. Rev. C **86**, 061301(R) (2012).
[11] Y. Fujiwara, M. Kohno, T. Fujita, C. Nakamoto, and Y. Suzuki, Nucl. Phys. A **674**, 493 (2000).
[12] S. A. Fayans, JETP Lett. **68**, 169 (1998).
[13] L. G. Cao, U. Lombardo, C. W. Shen, and N. V. Giai, Phys. Rev. C **73**, 014313 (2006).
[14] J. P. Jeukenne, A. Lejeune, and C. Mahaux, Phys. Rep. **25**, 83 (1976).
[15] M. Baldo, G. F. Burgio, H.-J. Schulze, and G. Taranto, Phys. Rev. C **89**, 048801 (2014).
[16] G. F. Bertsch, P. F. Bortignon, and R. A. Broglia, Rev. Mod. Phys. **55**, 287 (1983).
[17] M. Baldo, C. Maieron, P. Schuck, and X. Viñas, Nucl. Phys. A **736**, 241 (2004).
[18] W. Kohn and L. J. Sham, Phys. Rev. **140**, A1133 (1965).
[19] V. B. Soubbotin, V. I. Tselyaev, and X. Viñas, Phys. Rev. C **67**, 014324 (2003).
[20] J. Dobaczewski and J. Dudek, Phys. Rev. C **52**, 1827 (1995).
[21] Y. M. Engel, D. M. Brink, K. Goeke, S. J. Krieger, and D. Vautherin, Nucl. Phys. A **249**, 215 (1975).
[22] G. F. Bertsch and H. Esbensen, Ann. Phys. (NY) **209**, 327 (1991).
[23] E. Garrido, P. Sarriguren, E. Moya de Guerra, and P. Schuck, Phys. Rev. C **60**, 064312 (1999).
[24] M. Baldo, P. Schuck, and X. Viñas, Phys. Lett. B **663**, 390 (2008).
[25] P. Ring and P. Schuck, *The Nuclear Many Body Problem* (Springer-Verlag Edt. Berlin, 1980).
[26] R. R. Rodríguez-Guzmán, J. L. Egido, and L. M. Robledo, Phys. Rev. C **62**, 054319 (2000).
[27] J. L. Egido and L. M. Robledo, Lect. Notes Phys. **641**, 269 (2004).
[28] L. M. Robledo, HFBAXIAL computer code (2002).
[29] L. M. Robledo and G. F. Bertsch, Phys. Rev. C **84**, 014312 (2011).
[30] A. Arzhanov, T. R. Rodríguez, and G. Martínez-Pinedo, Phys. Rev. C **94**, 054319 (2016).
[31] Bao-An Li and Xiao Han, Phys. Lett. B **727**, 276 (2013).
[32] Xiao-Hua Li *et al.*, Phys. Lett. B **743**, 408 (2015).
[33] M. Wang *et al.*, Chin. Phys. C **36**, 1603 (2012).
[34] I. Angeli, At. Data Nucl. Data Tables **87**, 185 (2004).
[35] L. M. Robledo, M. Baldo, P. Schuck, and X. Viñas, Phys. Rev. C **77**, 051301(R) (2008).
[36] L. M. Robledo, M. Baldo, P. Schuck, and X. Viñas, Phys. Rev. C **81**, 034315 (2010).
[37] J. F. Berger, M. Girod, and D. Gogny, Nucl. Phys. A **428**, 23c (1984).
[38] S. A. Giuliani and L. M. Robledo, Phys. Rev. C **88**, 054325 (2013).
[39] S. A. Giuliani, L. M. Robledo, and R. Rodríguez-Guzmán, Phys. Rev. C **90**, 054311 (2014).
[40] M. Kortelainen, J. McDonnell, W. Nazarewicz, P.-G. Reinhard, J. Sarich, N. Schunck, M. V. Stoitsov, and S. M. Wild, Phys. Rev. C **85**, 024304 (2012).
[41] M. Warda, J. L. Egido, L. M. Robledo, and K. Pomorski, Phys. Rev. C **66**, 014310 (2002).
[42] G. F. Bertsch, W. Loveland, W. Nazarewicz, and P. Talou, J. Phys. G **42**, 077001 (2015).
[43] L. M. Robledo and G. F. Bertsch, Phys. Rev. C **84**, 054302 (2011).
[44] O. Bohigas, A. M. Lane, and J. Martorell, Phys. Rep. **51**, 267 (1979).
[45] T. Suzuki, Prog. Theor. Phys. **64**, 1627 (1980).
[46] E. Lipparini and S. Stringari, Phys. Rep. **175**, 103 (1989).